CED-3 caspase promotes dismantling but not onset of non-apoptotic linker cell death in *C. elegans*

Olya Yarychkivska[1,5], Lena M. Kutscher[1,2,5], Dana Mamriev[3], Betty Ortiz Bido[1], Yun Lu[1], Wolfgang Keil[4], Sarit Larisch[3], Shai Shaham[1,*]

[1]Developmental Genetics, the Rockefeller University, New York, USA

[2]Hopp Children's Cancer Center (KiTZ), Developmental Origins of Pediatric Cancer Group, German Cancer Research Center (DKFZ), D-69120 Heidelberg, Germany.

[3]Cell Death and Cancer Research Laboratory, Department of Human Biology and Medical Sciences, University of Haifa, 31905, Haifa, Israel.

[4]Institut Curie, Université PSL, Sorbonne Université, CNRS UMR168 Laboratoire Physico Chimie Curie, Paris 75005, France

[5]Equal contribution

[*]Correspondence: shaham@rockefeller.edu

ABSTRACT

Nuclear degradation accompanies cell death. To study this process, we followed nuclear dismantling of the *C. elegans* linker cell, which undergoes a non-apoptotic morphologically-conserved death program characterized by nuclear envelope crenellations and cell splitting. We show that although linker cell death is cell autonomous, nucleus elimination follows engulfment and is blocked in *rab-35* and *arf-6* phagosome maturation mutants. Surprisingly, although linker cell death is independent of the apoptotic caspase CED-3, CED-3 is partially required within the linker cell, and upstream of RAB-35 and ARF-6, for cell splitting, engulfment, and nucleus elimination. In parallel studies, we found that the kinase inhibitor staurosporine causes mouse embryonic fibroblasts to undergo caspase-independent non-apoptotic death accompanied by nuclear crenellations and, paradoxically, by *Caspase-3* activation. Our findings suggest mechanistic similarities between staurosporine-induced and linker cell death, revealing that, in some contexts, caspases do not initiate cell death but instead promote subcellular tasks required for cell clearance.

keywords: linker cell, linker cell-type death, LCD, caspase, non-apoptotic cell death, engulfment, degradation, *C. elegans*, mouse embryonic fibroblasts, MEF, staurosporine, nuclear crenellation, *ced-3*, *rab-35*, *arf-6*.

Introduction

Programmed cell death is a complex process that effects the destruction of cellular compartments and their building blocks [1-3]. How specific subcellular structures and organelles are destroyed during cell death is not well understood. Some aspects of cellular destruction appear to be cell autonomous. For example, during apoptosis, caspases acting within dying cells cleave regulatory proteins, leading to DNAse activation and subsequent chromatin dismantling and DNA degradation [4]. By contrast, caspase-dependent cleavage of Xk-family proteins results in presentation of cell surface lipids, such as phosphatidyl serine, attracting phagocytes that engulf the dying cell and promote its non-autonomous degradation [5, 6]. Indeed, once engulfed, the dying cell resides in a phagosome, which then fuses with lysosomes [2, 7]. Phagolysosomes in some contexts can tubulate into smaller vesicles whose subsequent degradation is more facile. In the degradation of *C. elegans* polar bodies, for example, tubulation requires the small GTPase ARL-8 acting in the engulfing cell, and depends on amino acid export, activation of the lysosomal mTOR complex, mTORC, and subsequent recruitment of a BLOC-1-related complex [8]. How dying cell organelles are dismantled within phagolysosomal tubules has not been extensively investigated, although it has been suggested that dying cell membrane breakdown is independent of autophagy [9].

Programmed cell death is a common cell fate during the development of the nematode *C. elegans*, with 131 of the 1090 cells born in the hermaphrodite undergoing this process [10, 11]. While most, if not all, of these cell death events are blocked by inhibiting the apoptotic caspase CED-3 [12, 13], the death of the male-specific linker cell is an exception [14]. The linker cell guides migration of the developing male gonad, and

its death, at the larva-to-adult transition, facilitates fusion between the *vas deferens* and the cloaca, generating an open reproductive system [15, 16] (Figure 1A). Linker cell death is non-apoptotic by morphological and genetic criteria [14, 17]. Unlike apoptotic cells, the dying linker cell fails to exhibit chromatin condensation. Indeed, even nuclear periphery-associated heterochromatin disappears during early stages of linker cell death [14]. While the nuclear envelope of apoptotic cells remains smooth as cell demise proceeds, the dying linker cell nuclear envelope is characterized by nuclear crenellations, deep invaginations that can be detected by both light and electron microscopy (Figure 1A) [3, 14, 18, 19]. Dying linker cells also exhibit swollen organelles, a feature reserved for only very late stages of apoptosis.

Genetically, linker cell death is independent of the main apoptotic caspase, CED-3, and of the three other caspase-related proteins encoded in the *C. elegans* genome [14, 17]. Linker cell death is also independent of other apoptotic effectors, including CED-4/Apaf1, CED-9/Bcl2, and EGL-1/BH3-only [14]. Instead, studies from our lab demonstrated that multiple upstream regulatory signals [14, 18-20] converge on the HSF-1 heat-shock factor, a transcriptional regulator that acts non-canonically to promote cell death instead of protecting against it [18]. During linker cell death, HSF-1 activates expression of target genes unrelated to the heat-shock response, including genes encoding the LET-70/UBE2D2 E2 ubiquitin ligase and other ubiquitin proteasome system components [18].

We previously showed that the linker cell undergoes stereotypical morphological changes as it dies [16]. Nuclear crenellation is followed by asymmetric cell splitting and subsequent engulfment of the resulting two fragments by different descendants of the U

progenitor cell, U.l/rp (Figure 1A). Degradation of the linker cell nucleus-containing fragment is mediated by the RAB-35 and ARF-6 small GTPases, which prepare the phagosome in which the linker cell fragment resides for lysosomal fusion and dismantling [16].

To understand how cellular organelles are degraded during cell death, we studied the process of nuclear dismantling in linker cell death. We show, using a combination of live confocal imaging and electron microscopy, that disassembly of the nuclear lamina and displacement of histones from the nucleus takes place downstream of linker cell splitting and phagosome maturation, and before nuclear envelope degradation. Although linker cell death does not require engulfment, we find that in *rab-35(lf)* or *arf-6(gf)* mutants, nucleus disassembly stalls. Surprisingly, a similar blockade is evident in *ced-3(lf)* caspase and *ced-4(lf)* Apaf1 mutants. While cell death is initiated in these mutants, and the linker cell is eventually degraded in many of them, about half of adult males exhibit a persisting unengulfed cell corpse even 24 hours later. We demonstrate that in *ced-3* mutants, cell splitting is defective, likely accounting for the engulfment defect. We also show that while the non-muscle myosin NMY-2 normally accumulates specifically in the smaller splitting fragment, it is more equally distributed between the two fragments in *ced-3* mutants.

Cell death induced by the non-specific kinase inhibitor staurosporine has been suggested to cause apoptosis; however, cell death ensues in cell lines established from the fetal thymus of mutants lacking key apoptotic effectors [21], suggesting a non-apoptotic mechanism. Indeed, we demonstrated that staurosporine-induced death of mouse embryonic fibroblasts (MEFs) is independent of *Casp3*, *Casp7, Bax, Bak and*

Tp53. Strikingly, fibroblast nuclei become crenellated, and expression of ubiquitin proteasome system components is induced, reminiscent of linker cell death.

Our studies suggest that back-and-forth signaling between the engulfing and dying cell may be necessary to trigger nuclear destruction during linker cell death; demonstrate a novel role for caspases in this cell death form; and suggest that linker cell-type death (LCD), in which caspases perform non-death auxiliary functions, may be conserved from *C. elegans* to mammals.

Results

Disruption of lamin and histone nuclear localization occurs after linker cell splitting and before nuclear membrane disassembly

To characterize nuclear dynamics during linker cell death, we imaged the localization of LMN-1 (the sole *C. elegans* nuclear lamin) endogenously tagged with GFP, as well as other reporter transgenes for the nuclear proteins HIS-24 (Histone H1), EMR-1 (Emerin), and NPP-1 (NUP54), in animals exhibiting different linker cell death stages. We found that while all these proteins are confined to the nucleus in animals in which the linker cell has not yet split, LMN-1, HIS-24, and NPP-1 take on a diffuse nucleocytoplasmic distribution in animals in which the linker cell has fragmented (Figure 1B-E, Supplemental Figure 1B). Localization of EMR-1 is less obviously disrupted, with at least some of the protein retaining what appears to be nuclear membrane association after linker cell splitting (Supplemental Figure 1A). None of these proteins are present in the small linker cell fragment generated after cell splitting.

To confirm these dynamics, we followed GFP::LMN-1 using a confocal long-term live-imaging microfluidic setup [22] in which linker cell death can be longitudinally followed in single animals. Corroborating our bulk time-course studies, we found that cell splitting precedes LMN-1 redistribution. The interval between these processes is variable (1 min to 3 h, n=7) but once initiated, LMN-1 diffusion occurs rapidly within 60-80 seconds (Figure 1F). GFP::LMN-1 dissociation coincides with nuclear envelope blebbing visible by brightfield imaging (Supplemental Figure 1C), which can serve as a proxy for lamina dismantling. Electron microscopy of a split cell undergoing nuclear blebbing reveals that nuclear membranes are intact despite lamina redistribution. (Figure 1G), consistent with partial retention of EMR-1 nuclear envelope localization (Supplemental Figure 1A).

Taken together, these studies demonstrate that nuclear dismantling during linker cell death is a multi-step process in which partial nuclear lamina disassembly and chromatin disruption follow cell splitting, while nuclear membranes are degraded only later.

Lamin disassembly during linker cell death requires phagosome sealing

Previous work showed that linker cell splitting coincides with engulfment of the two linker cell fragments by the two U.l/rp cells, a process we have termed competitive phagocytosis [16]. To assess the temporal relationship between phagosome formation and nuclear lamina disassembly, we examined by live imaging animals expressing GFP::LMN-1, *mig-24p*::iBlueberry to mark the linker cell, as well as an mKate2-PH reporter, derived from PLC-δ1 and expressed in linker cell engulfing cells. mKate2-PH marks unsealed phagosome membranes by binding to phosphatidylinositol (4,5)-bisphosphate (PI(4,5)P2) [16, 23, 24]. We found that when mKate2-PH signal is present around the linker cell,

revealing ongoing phagocytosis, GFP::LMN-1 remains localized to the nucleus (Figure 2A; note double membranes labelled by mKate2-PH corresponding to the engulfing cell plasma membrane and the forming phagosome membrane). Following mKate2-PH signal disappearance, signifying phagosome sealing (Figure 2B; only engulfing cell plasma membrane labelled), GFP::LMN-1 localization becomes diffuse (Figure 2C). Thus, phagosome sealing precedes linker cell nuclear lamina degradation. Of note, the time gap between mKate2-PH loss and GFP::LMN-1 redistribution is highly variable (2min, 15min, 30 min, 1h, 2h in the five animals we examined, Supplemental Figure 2), suggesting that phagosome sealing is unlikely to directly instruct nuclear lamina dismantling.

To further examine the connection between phagosome formation and linker cell nucleus degradation, we examined *rab-35(b1013)* GTPase mutants in which cell splitting is unperturbed but phagosome maturation fails to initiate [16]. While 76% of wild-type animals harboring a split linker cell also exhibit GFP::LMN-1 redistribution (n=38), only 2% of *rab-35(b1013)* mutants show localization changes (Figure 2D; n=50). Nuclear localization of GFP::LMN-1 is still evident in *rab-35(b1013)* mutants observed 24 hours after linker cell death onset (10/10 animals observed; Figure 2E). We previously showed that RAB-35 inhibits the ARF-6 GTPase by promoting its removal from the phagosomal membrane [16]. We found that *arf-6(ns388gf)* GTPase mutants, which have the same linker cell clearance defect as *rab-35(b1013)* mutants [16], are also unable to redistribute GFP::LMN-1 (0%, n=40; Figure 2D), and GFP::LMN-1 remains at the nuclear membrane even 24 hours after linker cell death initiation (Figure 2F). Thus, nuclear lamina

disassembly during linker cell death requires the RAB-35 phagosome maturation initiation factor acting through activation of ARF-6 [16].

CED-3 caspase and CED-4/Apaf1 promote linker cell degradation and nuclear lamina dismantling

To identify additional regulators of linker cell nuclear degradation, we examined the effects of mutations in known linker cell death and apoptosis genes at different time points during linker cell death. Consistent with previous findings [14], linker cell death is initiated normally in *ced-3(n2452)* mutants, where it is accompanied by nuclear crenellations and a reduction in cell volume. Unexpectedly, however, although the cell often acquires a rounded morphology, indicative of loss of attachment to neighboring cells, this change is delayed and sometimes absent in some animals (Figure 3E). Furthermore, we found that a linker cell corpse persists in 56% (n=114) of *ced-3(n2452)* mutants even 24 hours after cell death initiation (Figure 3A). We imaged these persisting linker cell corpses in animals carrying a *lag-2p*::GFP reporter labeling the linker cell and a *lin-48p*::mCherry reporter labeling the engulfing U.l/rp cells. In the few wild-type animals with remaining corpses, about half are engulfed; however, in *ced-3(n2452)* animals, most persisting cells are not engulfed (Figure 3B,C, Supplemental Movie 1).

We observed the same set of defects in *ced-3(n717)* mutants (49% persisting corpse, n=102), confirming that these are due to loss of CED-3 function (Figure 3A-C). Similar persisting cell defects were also observed in *ced-4*/Apaf1 mutants and to a lesser extent in *ced-9(n1950)* mutants carrying a gain-of-function mutation in the *ced-9*/Bcl2 gene (Figure 3A).

We used long-term live imaging of *ced-3(n2452)* animals, also containing a *mig-24*p::Venus linker cell reporter and a *lin-48*p::mKate2 engulfing cell reporter, to gain more insight into the temporal progression leading to the defects we observed (Supplemental movie 1). We found that development of the male tail, including tail tip retraction onset, appearance of first tail rays, and cuticle shedding, is normal in *ced-3(n2452)* animals (Supplemental Figure 3A-C). Likewise, lodging of the linker cell between the two engulfing U.l/rp cells and onset of nuclear crenellation are the same as in wild-type animals (Supplemental Figure 3D, E). However, linker cell rounding and splitting are delayed (Figure 3E,F), and the formation of the refractile nucleus-containing corpse is delayed as is its persistence time (Figure 3G,H). While small fragment clearance, when it occurs, is normal (Figure 3I), large fragment clearance often fails to take place (Figure 3J).

Importantly, in *ced-3(n2452)* and *ced-3(n717)* animals with persistent linker cell corpses, GFP::LMN-1 remains associated with the nuclear envelope (Figure 2D,G). This nuclear lamina degradation defect is similar to that of *rab-35(lf)* and *arf-6(gf)* mutants (Figure 2D-F). However, double mutants containing the *arf-6(gf)* mutation and either *ced-3(n2452)* or *ced-3(n717)* mutation have more severe linker cell clearance defects than either mutant alone, suggesting that *ced-3* acts, at least in part, in parallel to the RAB-35 pathway (Supplemental Figure 3G).

Together, our findings suggest that the apoptotic caspase CED-3 and its regulators, while not required for linker cell death per se, play auxiliary roles in linker cell degradation and nuclear lamina disruption.

CED-3 caspase and CED-4 Apaf1 are expressed and function in the linker cell

To determine the site of CED-3 action during linker cell degradation, we examined animals carrying a *ced-3p*::*ced-3-GFP* translational reporter. We found that GFP fluorescence is not evident in the migrating linker cell or in the U.l/rp engulfing cells. However, nuclear GFP puncta and diffuse cytoplasmic fluorescence are evident in the dying linker cell (Figure 4A). Linker cell-specific expression is also seen in animals carrying *ced-3*p::mCherry and *ced-3*p::GFP transcriptional reporters (Supplemental Figure 4A, B). Of note, GFP fluorescence is significantly lower compared to that seen in cells dying by apoptosis in the male tail (Supplemental Figure 4B), consistent with the notion that CED-3 plays a cell autonomous role in linker cell clearance. Expression of a *ced-4p*::*mKate2* transcriptional reporter is also detected in the dying linker cell (Figure 4B). However, unlike the *ced-3* reporter transgenes we examined, *ced-4*p::*mKate2* is expressed in both the migrating and dying linker cell (Figure 4B). Thus, *ced-3* and *ced-4* may function in the linker cell for its clearance.

To further test this idea, we used linker cell-specific RNAi to inhibit CED-3 expression and found significant linker cell corpse persistence 24 hours after linker cell death initiation (Figure 4C). Furthermore, expressing *ced-4* cDNA under the control of the *mig-24p* linker cell-specific promoter rescues the linker cell clearance defect of *ced-4(n1162*) mutants; but expressing *ced-4* using the *lin-48p* engulfing cell promoter does not (Figure 4D).

Our functional studies and expression results, therefore, demonstrate that *ced-3* and *ced-4* act cell autonomously within the linker cell to promote its clearance.

CED-3 is required for linker cell splitting and NMY-2/type II myosin shunting into the small fragment

While imaging *ced-3(n2452)* mutants with our long-term imaging setup, we noted that linker cell splitting into two fragments is significantly prolonged (Figure 3F), with the two fragments often connected by a long cellular bridge (Figure 5A). Furthermore, while splitting eventually proceeds to completion in some animals, in others the two fragments remain connected for hours (Figure 5D-F; n=3/5 animals). Consistent with these findings, imaging a synchronized population of *ced-3(n2452)* males at different timepoints reveals a significant proportion of animals with linker cell fragments connected by an unsevered bridge. This is markedly different from a similarly synchronized wild-type male population, in which linker cell splitting is rarely observed, suggesting that it is normally a rapid process (Figure 5B,C; [16]).

Cell splitting and nuclear lamina dismantling are hallmarks of mitotic cell division, raising the possibility that linker cell fragmentation may result from an atypical cell division. To test this, we performed a candidate RNAi screen against cell cycle and other mitotic regulator genes (16 cell cycle genes, 71 total). We found no effect on linker cell death initiation in any of these. However, RNAi against several candidates, including *plk-1*, *cye-1*, *nop-1* and *nmy-2*, results in cell clearance delay in animals scored 8h after the larva-to-adult molt (Supplemental Figure 5A). When examining animals expressing an endogenously tagged NMY-2::GFP, marking a type II myosin required for contractile ring formation during cytokinesis [25, 26], we noticed sequestering of GFP fluorescence to the small fragment during linker cell splitting (Figure 5G,H, n=16). By contrast, in *ced-3*(*n2452*) animals, NMY-2::GFP fluorescence is evident in both fragments and localizes near and

within the connecting cellular bridge (Figure 5I, n=9/13). During mitosis microtubules assemble into spindles. Interestingly, we also observed microtubule reorganization during LCD, visualized by a tubulin TBA-1::TagRFP reporter; however, instead of forming spindles, microtubules form condensed puncta (Supplemental Figure 5B-E').

We conclude, therefore, that CED-3 caspase is required for linker cell splitting and NMY-2 redistribution, and that failure of these events may account for the subsequent defects in linker cell engulfment and nuclear lamina degradation. Our results also raise the possibility that linker cell death may be accompanied by an atypical form of cell division.

Mouse embryonic fibroblasts treated with staurosporine undergo non-apoptotic cell death reminiscent of linker cell death

Staurosporine (STS), a non-specific kinase inhibitor [27], has been suggested to induce apoptosis in cultured cells [28, 29]. However, staurosporine-treated immortalized fetal thymocytes from mice lacking *Apaf1*, *Casp9*, *Casp8*, or *Bax* and *Bak* still die, and death is accompanied by caspase 3 processing [21], suggesting possible similarities with linker cell death. To test this, we generated embryonic fibroblasts from wild-type, *Casp3; Casp7*^{DKO}, *Bax;Bak*^{DKO} and *Tp53*^{KO} mice, treated them with STS, and assessed nuclear morphology by electron microscopy. Remarkably, wild-type and mutant cells alike display crenellated nuclei, starting already 30 minutes after STS exposure (Figure 6A-H), with this proportion increasing dramatically over time (Figure 6I). These findings, therefore, raise the possibility that the mechanism driving linker cell death in *C. elegans* may also promote cell death in mammalian settings.

To assess this idea further, we performed RNAseq on wild-type fibroblasts at 30 min following exposure to STS and compared to DMSO-treated wild-type fibroblasts. Although few genes are transcriptionally induced at early timepoints, when nuclear crenellation is already evident, those that are induced include ubiquitin proteasome system E3 ligase components (*Tdpoz4, Tdpoz8, Spopfm2*). These findings raise the possibility that molecular aspects of STS-induced linker cell-type death may be shared with *C. elegans* linker cell death, and that nuclear changes seen in these two processes are both morphologically and molecularly similar.

Discussion

CED-3 may have a primary role in linker cell splitting

The findings described in this study are consistent with a model in which non-apoptotic death of the *C. elegans* linker cell requires components of the apoptotic machinery, including the principal caspase, CED-3, to execute auxiliary tasks that contribute to the fidelity of dying cell degradation. Indeed, loss of CED-3 caspase leads to defects in linker cell splitting, in linker cell rounding, indicative of abnormally maintained adhesion to neighboring cells, in linker cell corpse engulfment, and to an inability to execute nuclear degradation. Do these defects reflect independent functions of CED-3 caspase, or might they be related?

The earliest linker cell degradation defect we observe in *ced-3* mutants is the inability to efficiently split the cell into a large and a small fragment (Figure 7). This defect correlates with abnormal distribution of non-muscle myosin NMY-2, which instead of concentrating primarily in the small fragment aberrantly localizes to both fragments near

the presumptive scission site. Our findings support the notion that all other defects we observe in *ced-3* mutants could stem from this initial cell splitting abnormality. As we previously demonstrated, linker cell splitting occurs concomitantly with engulfment of each linker cell fragment by a different engulfing cell, either U.lp or U.rp, through competitive phagocytosis [16]. We posit that a defect in linker cell fragment separation, leading to persistence of a fragment-joining bridge, forms a physical barrier that prevents engulfing cells from fully surrounding each linker cell fragment (Figure 7). This, in turn, prevents formation of a sealed phagosome. As we show, phagosome sealing is likely a pre-requisite for nuclear dismantling, as mutants that prevent early stages of phagosome maturation fail to dismantle the linker cell nucleus. Thus, the persistence of an intact nucleus in *ced-3* mutants is likely an indirect consequence of a defect in linker cell splitting (Figure 7).

Is linker cell death a consequence of a failure in cell division?

Caspases carry out numerous non-apoptotic tasks. In *C. elegans*, for example, CED-3 controls p38 MAPK activity during larval development [30]. Caspases also ensure the fidelity of cell division. Mammalian Caspase 2, for example, is important for cell cycle progression in mouse embryonic fibroblasts [31], and Caspase 4 promotes epithelial cell division by controlling actin polymerization [32]. Other caspases have also been suggested to control mitosis [33]. These observations raise the intriguing possibility that linker cell splitting, which requires CED-3 caspase activity, is mechanistically related to cell division. Our findings are consistent with this idea. Nuclear lamina degradation, for example, is a common feature of both mitosis and linker cell death [34]. In addition,

localization of non-muscle myosin to the cytokinetic furrow in mitotically dividing cells and to the linker cell scission site may reflect similar functions [35]. Reorganizing of tubulin also occurs during mitosis and, in a different way, in linker cell death. Furthermore, as in many other non-apoptotic roles for caspases, the level of caspase expression in non-apoptotic settings including cell division is around an order of magnitude lower than in dying cells [36-38]. The same is true, as we describe here, in the linker cell.

The juxtaposition of an apoptotic caspase, CED-3, with a non-apoptotic role in cell division, during a non-apoptotic cell death process, LCD, is intriguing and may point to the evolutionary origins of LCD and apoptosis. In one model, LCD may be an ancient cell death program activated by a failure in cell division, a process that was perhaps once primarily governed by caspases. As redundant cell division mechanisms arose, caspases were instead co-opted to play a more central role in cell death, leading to the development of apoptosis. Caspase-dependent apoptotic cell death appears to be a much more efficient process than LCD [2], supporting an evolutionary incentive to favor a role for these cysteine proteases in cell death.

Is the linker cell-type death mechanism conserved in mammals?

We previously published a survey of electron micrographs demonstrating that cell death accompanied by nuclear crenellations is commonplace in vertebrate development and in disease [3]. Our finding that MEFs undergo a similar morphological change in response to treatment with the cell-death inducer and kinase inhibitor staurosporine adds to this notion. Although our findings suggest involvement of ubiquitin proteasome system factors early on in staurosporine-induced death, whether these factors are functionally required

for LCD remains to be determined. Nonetheless, the ability of cell death to proceed in *Casp3/7*, *Bax/Bak*, and *Tp53* knockout cells suggests molecular similarities with linker cell death. Disruption of these and other genes identified in our RNAseq studies may reveal the extent of molecular conservation with *C. elegans* linker cell death.

Acknowledgements

Some strains were provided by the CGC, which is funded by the NIH Office of Research Infrastructure Programs (P40 OD010440). This work was supported by NIH NRSA Training Grant GM066699 to L.M.K., NIH K99GM151467 to O.Y., and NIH grants R35NS105094 and R01HD103610 to S.S.

Author contributions

Conceptualization, O.Y, L.M.K. and S.S.; Methodology, O.Y, L.M.K., W.K., B.O.B., D.M., Y.L., S.L. and S.S.; Software, W.K.; Formal Analysis, O.Y., L.M.K.; Investigation, O.Y, L.M.K., W.K., B.O.B., D.M., Y.L.; Writing – Original Draft, O.Y. and L.M.K.; Writing – Review & Editing, O.Y., L.M.K., W.K., S.L. and S.S.; Funding Acquisition, O.Y., L.M.K., W.K., and S.S.; Resources, O.Y., L.M.K., W.K., B.O.B. and S.S.; Visualization, O.Y., L.M.K., W.K.,Y.L. and S.S.; Supervision, S.L. and S.S.

Materials and Methods

Key reagent table.

Resource	Source

nsIs589: UV/TMP integration of *nsEx5123* (pLMK09[*lin-48p::mKate2*)[7] (10 ng/ul), *unc-119*(+) 25 ng/ul, pBluescript (65 ng/ul)]	PMID: 28041904
bcIs109: *ced-3p::ced-3-GFP*, rol-6(+),	gift from B. Conradt, PMID: 26657541
nsEx5307: pLMK65(*ced-4p::mKate2*) (25 ng/ul) + *unc-119*(+) (25 ng/ ul) + pBluescript (50 ng/ul)]	This study
nsEx5627,-8,-9: pLMK66(*mig-24p::ced-4a* cDNA) (20 ng/ul) + *odr-1p::RFP*(+) (20 ng/ul) + *pEB30* (20 ng/ul) + pBluescript (40 ng/ul)	This study
nsEx5619,-20,-81: pLMK67(*lin-48p::ced-4a* cDNA-SL2-mCh) (20 ng/ul) + *odr-1p::RFP*(+) (20 ng/ul) + pBluescript (60 ng/ul)	This study
nsIs495: UV/TMP integration of *nsEx4360*(*lin-48*p::*mCherry* (25 ng/ul)+ pBluescript (75 ng/ul))	This study
nsIs25: *ced-3p::GFP, rol-6*(+)	gift from C. Maurer, PMID: 17329362

nsEx4944: *pPG08*(*ced-3p::mCherry*) (10 ng/ul) + *unc-119*(+) (25 ng/ul) + pBluescript (65 ng/ul)	gift from P. Ghose
nsIs653: UV/TMP integration of *nsEx5304*(*lin-48*p::*mKate2-PH* (25 ng/ul)+ pBluescript (75 ng/ul))	PMID: 28041904

C. elegans

C. elegans strains were raised at 20°C on nematode growth medium (NGM) seeded with OP50 bacteria, unless otherwise indicated. Wild-type animals were of the Bristol N2 strain. All strains have one mutation that generate a high incidence of male progeny, *him-5*(*e1490*) V. Transgenic lines were generated by injection of plasmid DNA mixes into the hermaphrodite gonad. Integrated transgenic strains were generated with UV/trioxalen treatment (Sigma, T6137) [39] and were outcrossed at least four times before imaging experiments. Most strains also had one of three integrated linker cell markers *nsIs763*(*mig-24p::*iBlueberry) II*, qIs56*(*lag-2*p::GFP) V, *nsIs65(*[*mig-24*p::Venus) X, or *nsIs650(*[*mig-24*p::mKate2) X. Other alleles are as follows:

LGI

lmn-1(jf98), nmy-2(cp13), tba-1(pg77)

LGII

bqSi142 (*emr-1p*::emr-1::mCherry + unc-119(+));

LGIII

ced-9(n1950), ced-4(n1162), rab-35(*b1013*), *rab-35*(*tm2058*), *tbc-10*(*gk388086*), *unc-119*(*ed3*)

LGIV

ced-3(n717), ced-3(n2452), arf-6(*tm1447*), *arf-6*(*ns388*)

LGV

egl-1(*n1084n3082*)

LGX

stIS10116(*his-72p*::his-24::mCherry::let-858 3'UTR)

Germline Transformation and Rescue Experiments

Plasmid mixes containing the plasmid of interest, co-injection markers, and pBluescript were injected into both gonads of young adult hermaphrodites (PMID: 8531738). Injected animals were singled onto NGM plates and allowed to grow for two generations. Transformed animals based on co-injection markers were picked onto single plates, and screened for stable inheritance of the extrachromosomal array. Only lines from different P0 injected hermaphrodites were considered independent. For cell-specific rescue experiments, animals expressing fluorescence protein in either the linker cell or the U.l/rp cells were picked to a new plate at the early L4 stage, before linker cell death, to avoid bias. Isolated animals were then staged based on tail morphology under a white light microscope for appropriate linker cell scoring.

Linker Cell Survival and Corpse Persistence Assays

Linker cell death was scored as previously described [19]. Briefly, unstarved gravid hermaphrodites were bleached to isolate embryos, which were allowed to hatch overnight in M9. Synchronized L1 animals were released on 9-cm NGM plates seeded with OP50 or HT115 E. coli containing the RNAi construct of interest on IPTG-RNAi plates. Male animals were isolated onto a new plate prior to the L4-to-adult transition based on full retraction of the male tail tip with rays visible under the unshed L4 cuticle. 2h later (linker cell survival) or 24h later (corpse persistence), these animals were mounted onto 2% agarose-water pads, anaesthetized in 25 mM sodium azide, and examined on an Axioplan 2 fluorescence microscope (Zeiss) with a 63x/1.4NA objective (Zeiss) and Nomarski optics. The linker cell was identified by location, morphology, and fluorescence from reporter transgenes. Cells were then scored as surviving, dead, or gone based on DIC morphology and fluorescence.

Linker cell-specific RNAi

RNAi was performed by feeding using a linker cell-specific RNAi strain [18]. Gravid hermaphrodites were bleached and the released embryos were synchronized at the L1 stage by leaving them overnight in M9. L1 animals (30% of which were male) were added to each RNAi plate and grown for approximately 48 hrs at 20˚C. Animals were picked at the L4-adult molting stage and 8 hr adults were scored using a fluorescence dissecting scope (Leica). Clones were from the Ahringer feeding library [40].

Electron Microscopy

2h adult males with a linker cell GFP marker were mounted on 2% agarose/M9 pads and lightly anesthetized with 25mM sodium azide, then observed under a fluorescence dissecting microscope or by DIC microscopy to determine the approximate stage of linker cell death. Split stage accompanied by lamina dissociation was verified by the presence of perinuclear blebbing (Supplemental Figure 1C). Animals were then fixed, stained, embedded in resin, and serially sectioned using standard methods [41]. MEFs were grown on grids in standard media. Before and after STS treatment, they were fixed, stained, embedded and serially sectioned using standard methods.

Serial images were acquired using a Titan Themis 200 kV transmission electron microscope with Cs Image Corrector. Image processing and analysis were performed using ImageJ and IMOD software.

Confocal Imaging

Confocal images were acquired using a Zeiss LSM 900 inverted laser scanning confocal microscope with a 63x/1.4 NA oil objective. Animals were immobilized in 200 mM sodium azide either on 1% agar pads or using microfluidic devices [22].

Long-Term Imaging and Movie Generation

Early L4 male animals were imaged in a microfluidic device [22] for Figures 1F, 2A-C, 3E-J, S3C-H, and 5D-F. Animals were fed a constant flow of NA22 bacteria in S medium, supplemented with kanamycin (50 ng/µl) to prevent bacterial overgrowth. Animals were immobilized and imaged every 8 minutes for at least 20h. Mutant animals were typically imaged for > 30h. Exposure time and light intensity was held constant across strains when

the same integrated transgene was imaged. Occasionally tail development was perturbed by the flow of medium and repeated immobilization procedures, and these animals were not included in subsequent analyses.

Confocal long-term imaging was performed manually (Figures 1F, 2A-C) over 10-12h. Animals were immobilized every 30 minutes to check the stage of the linker cell. Images were taken more frequently around the stages of interest. Exposure time and light intensity were held constant.

Deconvolution

Used Hyugens Pro with theoretically calculated PSF, all auto options, except the number of iterations was increased to 200.

Image Analysis

For long-term imaging: Image analysis was performed using custom-written MATLAB R2016b (Mathworks) scripts. To overlay imaging frames, we straightened each three-dimensional image stack using a previously published algorithm (PMIDs:28041904, 18025002) based on a manually selected worm backbone in the DIC channel. To correct for small residual animal movements during multi-channel acquisition, obvious landmarks visible in the fluorescence channels, such as the cloaca, fluorescently labeled cells in the animal's tail, or vesicles within the U-cell descendants were then manually aligned to the DIC channel in each frame. Time-lapse movies were generated by centering all straightened, aligned images on the linker cell and cropping the entire movie to an

appropriate size. Frames were removed from the movies whenever residual animal movement excessively blurred the images.

For regular confocal: Images were processed using Imaris version 10.12.0.

Plasmid Construction

Plasmids containing *lin-48*p, *mig-24*p, or transcriptional reporters were cloned using multi-piece one-step cloning into a modified pPD95.75 backbone lacking GFP.

Quantification and Statistical Analysis

Statistical analysis was performed using GraphPad Prism. Statistical parameters including mean ± standard error of the proportion, mean ± SEM, and n are reported in the main text, figures and figure legends. Data is judged to be statistically significant when $p < 0.05$ by Fisher's exact test or student's t-test, where appropriate.

Genetic Data Analysis

When comparing a transgenic line to the parental strain, a minimum of three independent lines was scored. Approximately 100 animals from each of these lines were examined for linker cell defects, and compared to the parental strain using a Fisher's exact test to determine significance. For ease of presentation, we pooled the lines from a given experiment and displayed them on the relevant figure using mean ± SEM (N = 3, 4, or 5 lines).

Cell Culture and reagents.

MEF cells were grown in complete DMEM medium (1% sodium pyruvate, 1% L-glutamate, 1% Pen-strep and 10% fetal bovine/calf serum) at 37°C. Staurosporine (STS) was purchased from Fermentek (cat#62996-74-1.5).

Data and Software Availability

Custom image analysis scripts are available upon request.

FIGURE LEGENDS

Figure 1. Nuclear dismantling initiates at the split stage of LCD.

(A) Stages of linker cell death (LCD) that ensures after the cell arrives at the tail.

(B) Representative confocal images of endogenous reporter for lamin during the stages of competitive phagocytosis and splitting.

(C) Quantification of cells with diffuse lamin signal at two stages. The number of animals scored inside bars. Average of 3 independent experiments. Error bars, standard error of the proportion or standard error of the mean. n.s., $p > 0.05$, Fisher's exact test.

(D) Representative confocal images of HIS-24 (histone H1) during the stages of competitive phagocytosis and splitting.

(E) Quantification of cells with diffuse histone signal at two stages. The number of animals scored inside bars. Average of 3 independent experiments. Error bars, standard error of the proportion or standard error of the mean. n.s., $p > 0.05$, Fisher's exact test.

(F) Long-term confocal imaging of GFP::LMN-1 in a single animal showing rapid lamina redistribution.

(G) Electron micrographs of linker cells at a competitive phagocytosis and split stages.

Figure 2. Lamina disassembly takes place upon phagosome maturation at the split stage and is blocked in *rab-35*, *arf-6* and *ced-3* mutants.

(A) Confocal live-imaging of a linker cell labeled with mig-24p::iBlueberry, lamin endogenously tagged with GFP, and mKate2-PH labeling unsealed phagosome membranes and plasma membrane of the engulfing cells. Asterisk demarks the intact lamina of the linker cell nucleus. Arrowhead points to the unsealed phagosome membrane. Arrow points to the engulfing cell membrane. Triangle is at the site of deformed nuclear lamina.

(B) Arrowhead shows the disappearance of the unsealed phagosome signal, while asterisk shows that the linker cell lamina is still intact. Triangle is at the site of deformed nuclear lamina.

(C) Linker cell lamina is diffuse 2 minutes later as GFP signal is seen to colocalize with iBlueberry. Arrow points to the engulfing cell membrane. Inset shows GFP signal alone.

(D) Quantification of % linker cells with diffuse lamina at the split stage in WT and *rab-35(b1013)*, *arf-6 (ns388)*, *ced-3(n2452)* and *(n717)* mutants. The number of animals scored inside bars. Average of 2 or 3 independent experiments. Error bars, standard error of the proportion or standard error of the mean. n.s., $p > 0.05$, Fisher's exact test.

(E, F and G) Confocal imaging of lamina status using endogenously tagged GFP::LMN-1 reporter in persisting linker cells labeled by *mig-24*p::mKate2 in 24h old adults in *rab-35(b1013)*, *arf-6 (ns388)*, *ced-3(n2452)* mutant animals. Scale bar, 2 μm(E,G), 1 μm (F).

Figure 3. ced-3 mutant animals exhibit an engulfment and LCD progression defects.

(A) Linker cell degradation in indicated genotypes. Strains contain either *lag-2p::GFP* linker cell reporter or *nsIs1(lag-2p::GFP, rol-6(+))* (denoted by ^) and *him-5(e1490).* Number of animals scored inside bars. Error bars, standard error of the proportion. Fisher's exact test.

(B) Majority of persisting linker cells in 24h adults are unengulfed in *ced-3(n2452)* and *(n717)* mutants. All strains carried *lin-48p*::mCherry reporter marking engulfing cells, *lag-2p*::GFP marking linker cells. Scoring was performed on a confocal microscope.

(C and D) Representative confocal images of unengulfed linker cells in 24h adults in *ced-3(n2452)* and *(n717)* mutants. *lin-48p*::mCherry reporter marks engulfing cells, *lag-2p*::GFP marks linker cells.

(E-J) Quantification of long-term live-imaging of *ced-3*(*n2452*) animals. Strains contain linker cell reporter (*mig-24p::Venus*), U.l/rp cell reporter [*lin-48p::mKate2*], and *him-5*(*e1490*) to enrich for males. Dots, individual events in single animals in min with respect to first contact. X, event did not occur and was not factored into statistical analysis. Bars, mean ± std. n.s., p>0.05, Student's t-test. Wild type (WT) are same animals as in [16].

Figure 4. CED-3 and CED-4 are expressed in the linker cell and function cell-autonomously.

(A) *ced-3* translational reporter expression and localization. Linker cell outlined in green, animal outlined in white. Solid line indicates position of the cloaca.

(B) *ced-4* transcriptional reporter expression. Linker cell outlined in green, animal outlined in white. Solid line indicates position of the cloaca.

(C) Scoring of persistent linker cells in 24h adults in a linker cell-specific RNAi strain treated with control or *ced-3* RNAi. The number of animals scored inside bars. Average of three independent experiments. Error bars, standard error of the proportion or standard error of the mean. n.s., p > 0.05, Fisher's exact test.

(D) Linker cell degradation in indicated genotypes. Strains contain *lag-2*p*::GFP* linker cell reporter and *him-5*(*e1490*). UCp, *lin-48*p. LCp, *mig-24*p. Number of animals scored inside bars. Average of at least three independent lines. Error bars, standard error of the proportion or standard error of the mean. Fisher's exact test.

Figure 5. ***ced-3* linker cells exhibit a splitting defect and NMY-2 mislocalization**

(A) *ced-3(n2452)* LCs exhibit the "almost split" morphology, where the two fragments are joines by a long bridge.

(B) Timeline of LC stages in wild-type animals starting at the molting stage, when majority of LCs are dying.

(C) Timeline of LC stages in *ced-3(n2452)* animals having a significant proportion of "almost split" cells during all of the timepoints.

(D-F) Long-term live imaging of a single LC large fragment (z14) and small fragment (z18) displaying the "almost split" morphology for 2.5h.

(G-H) Confocal imaging of NMY-2::GFP endogenous reporter showing NMY-2 localization to the small anuclear fragment.

(I) *ced-3(n2452)* LC exhibits a symmetric NMY-2 localization around the scission site.

Figure 6. **Mouse embryonic fibroblasts (MEFs) acquire LCD hallmark nuclear deformations in a caspase-independent manner upon treatment with staurosporine (STS).**

(A-H) Ultrastructural details of wild-type and apoptotic mutant MEFs treated with STS. Arrows denote nuclear deformations.

(I) Quantification of cells acquiring nuclear deformations 0.5 and 3 hours after STS treatment.

Figure 7. Model for CED-3 function in linker cell removal.

In wild-type, linker cells undergo splitting, followed by lamina disassembly and accompanied by asymmetric NMY-2 redistribution to the small anuclear fragment. LC is engulfed and fully degraded. In *ced-3* (-), the splitting is stalled, NMY-2 is localized to both fragments and to the bridge between the two fragments. This results in failure of engulfment and nuclear dismantling, yielding persisting cells.

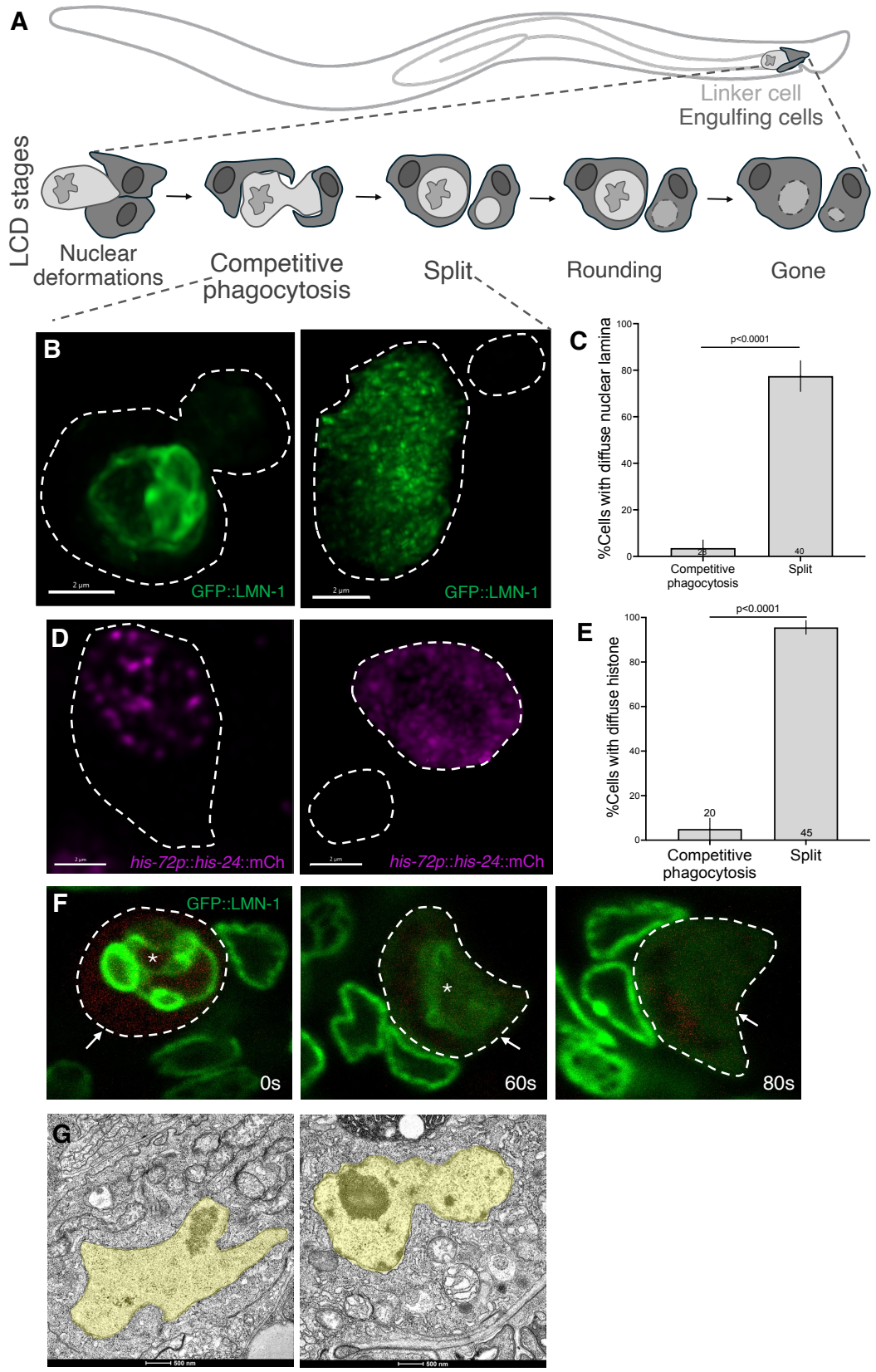

Figure 1. Nuclear dismantling starts at the split stage of LCD.

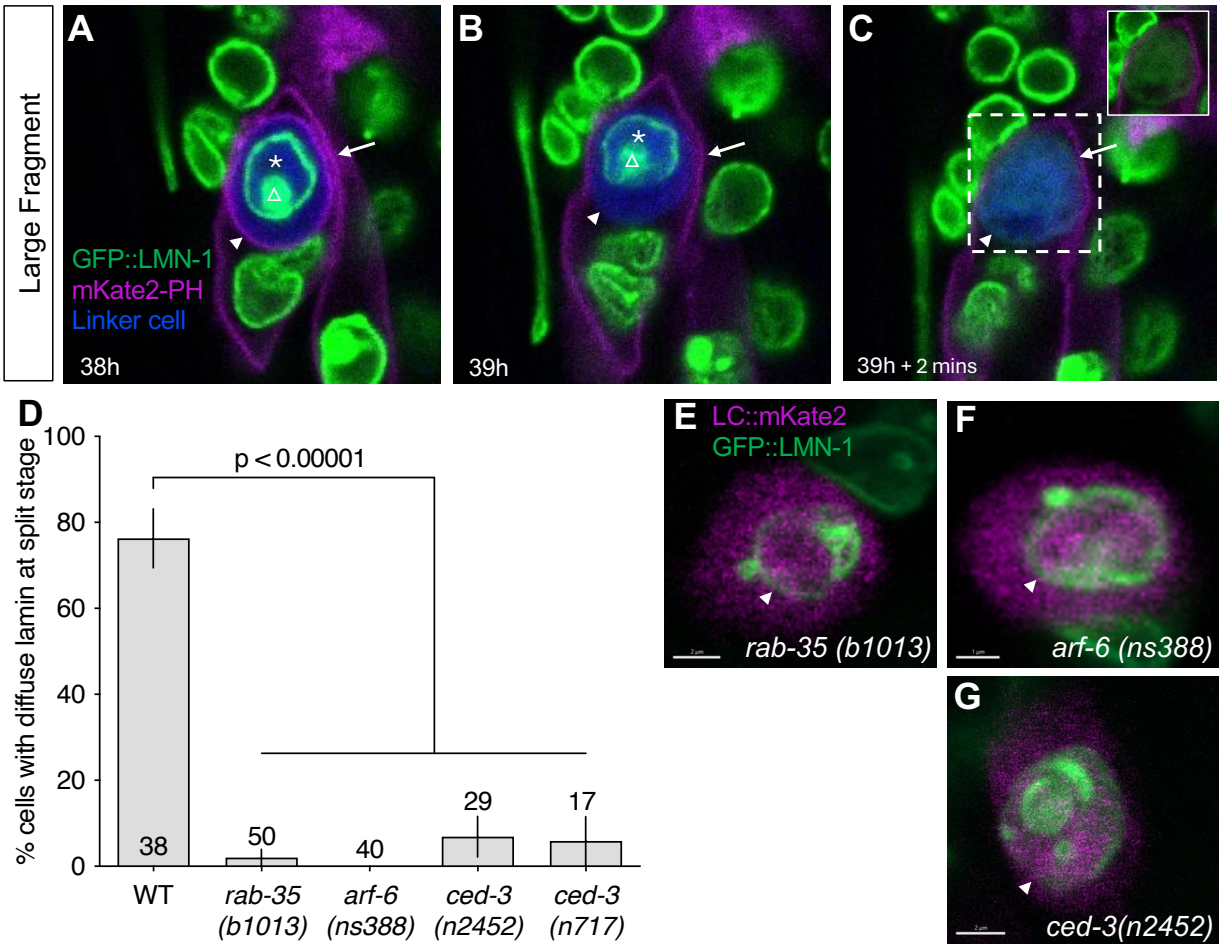

Figure 2. Lamina disassembly takes place upon phagosome maturation at the split stage and is blocked in *rab-35*, *arf-6* and *ced-3* mutants.

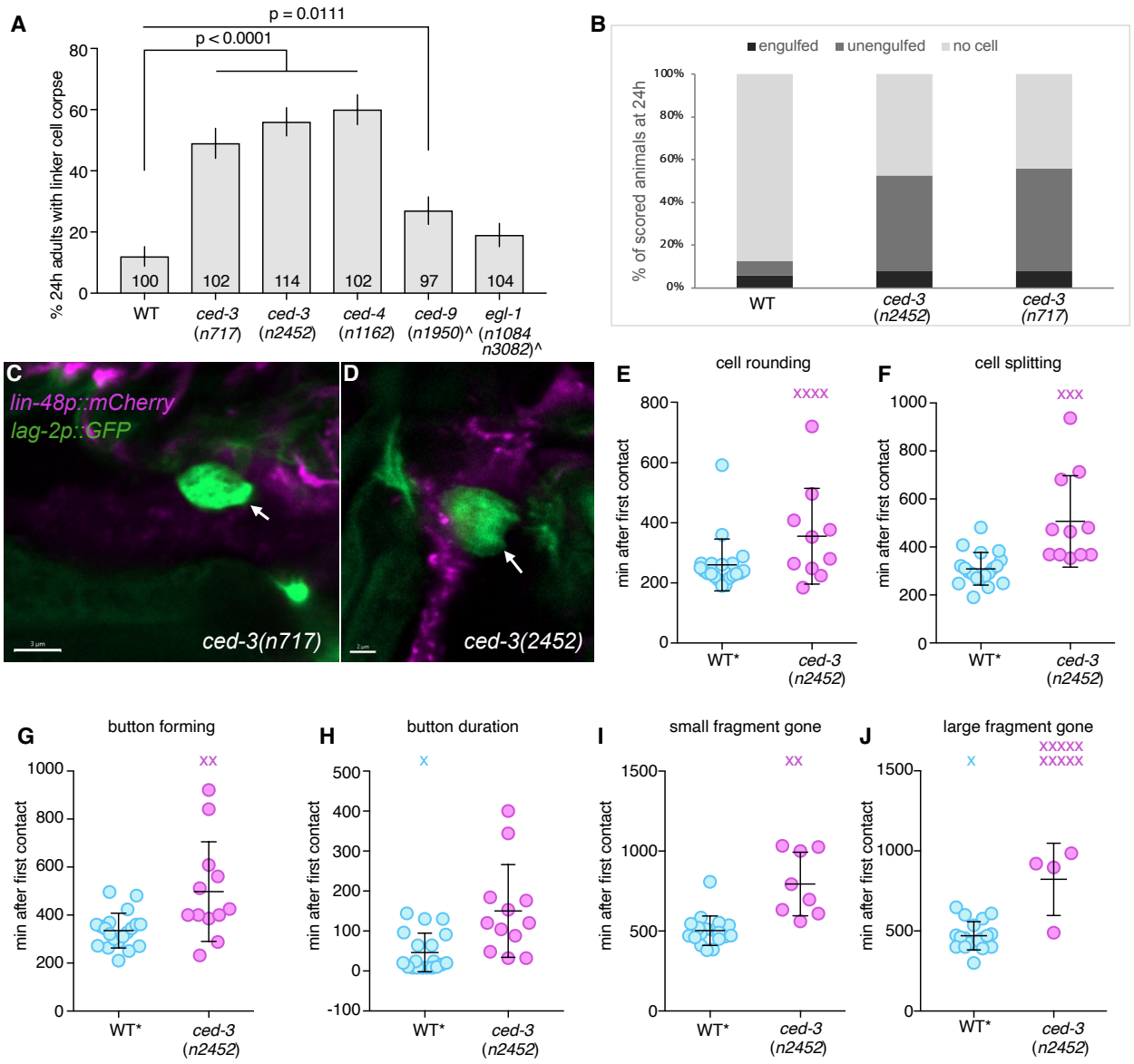

Figure 3. *ced-3* mutant animals exhibit an engulfment and LCD progression defects.

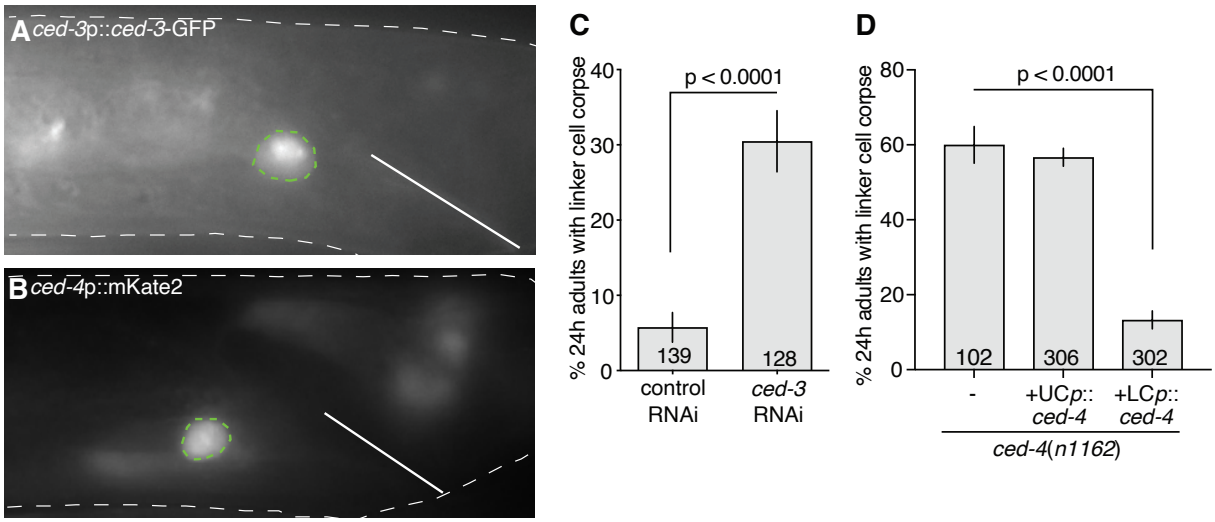

Figure 4. CED-3 and CED-4 are expressed in the linker cell and function cell-autonomously.

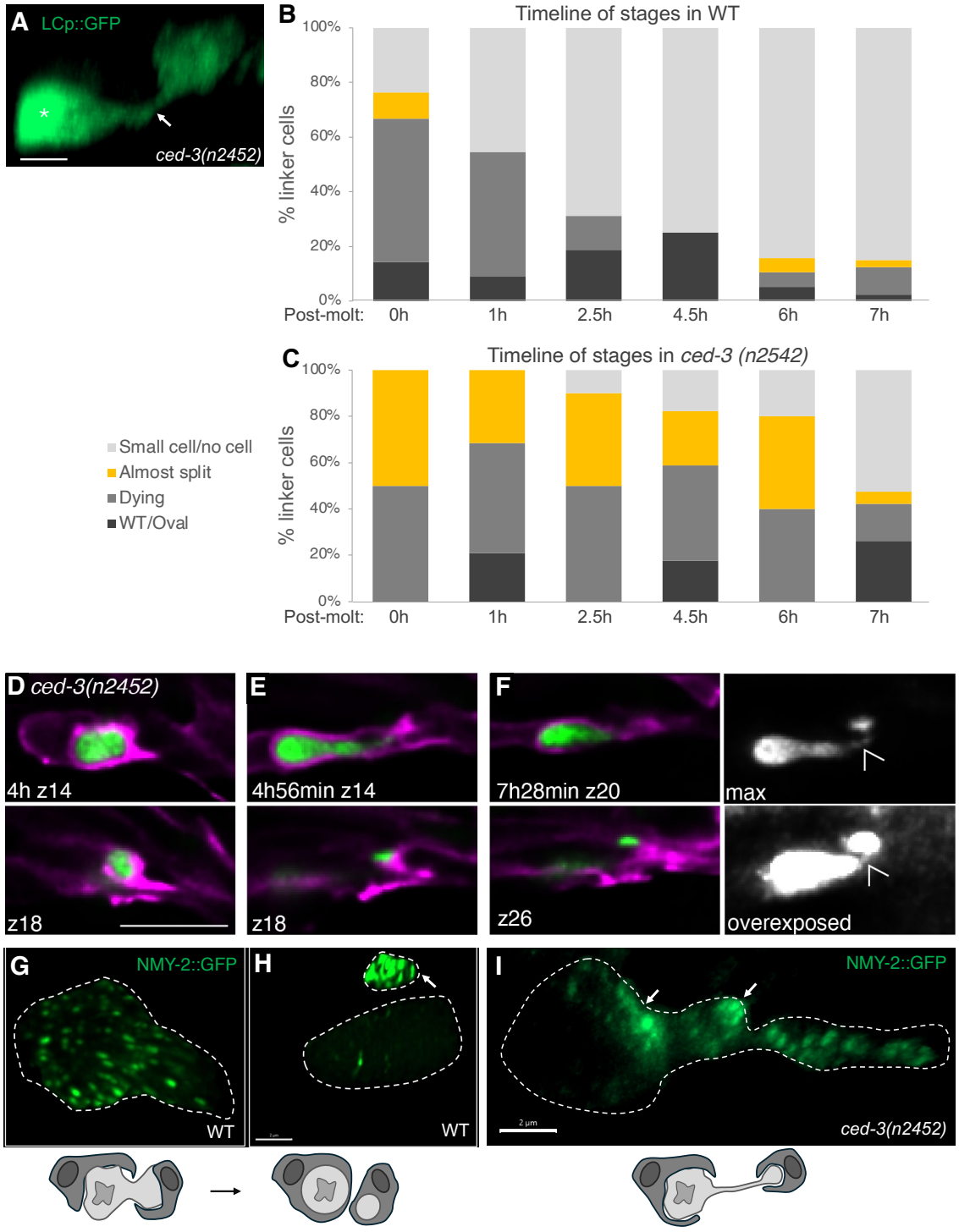

Figure 5. *ced-3* linker cells exhibit a splitting defect and NMY-2 mislocalization.

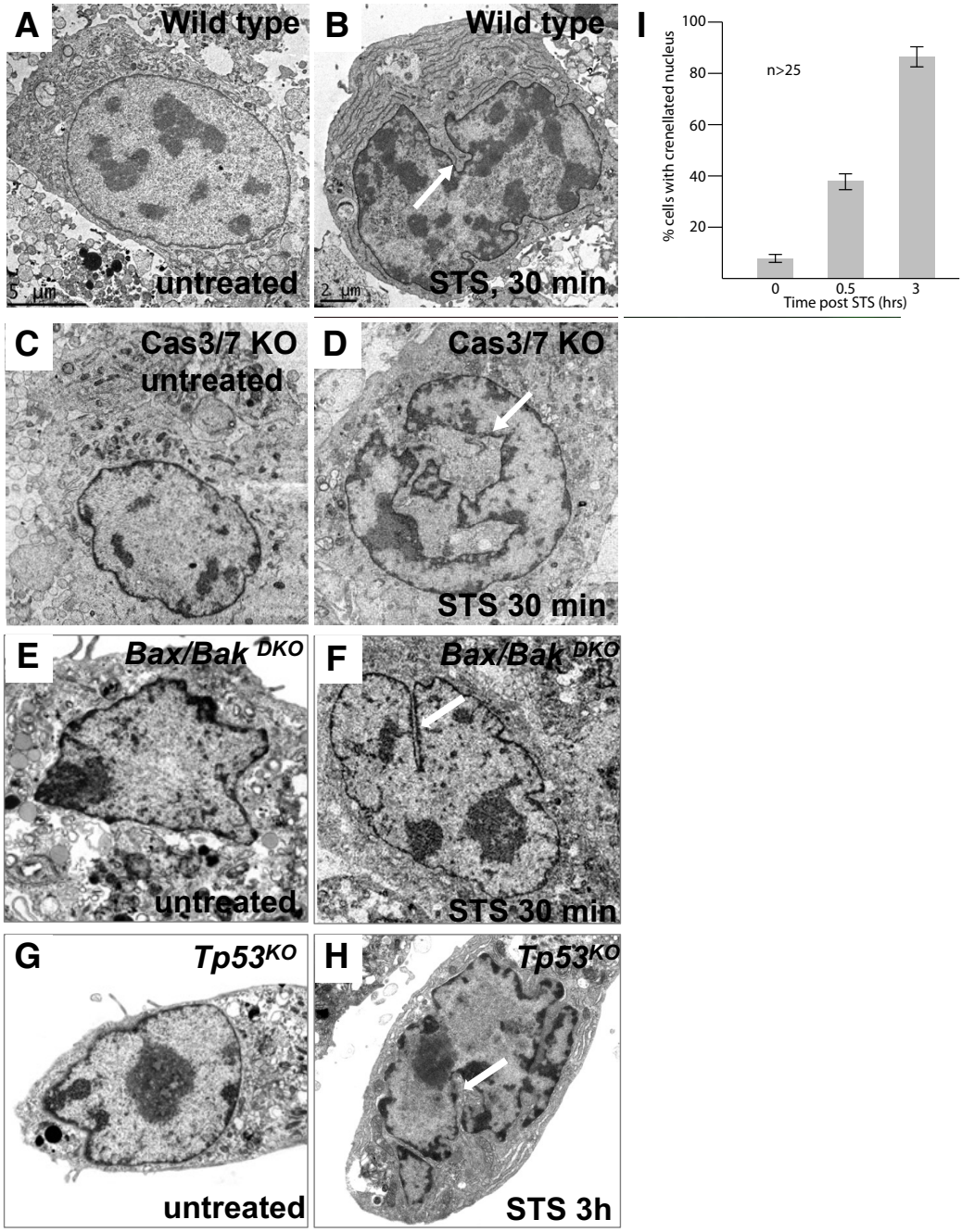

Figure 6. Mouse embryonic fibroblasts (MEFs) acquire LCD hallmark nuclear deformations in a caspase-independent manner upon treatment with staurosporine (STS).

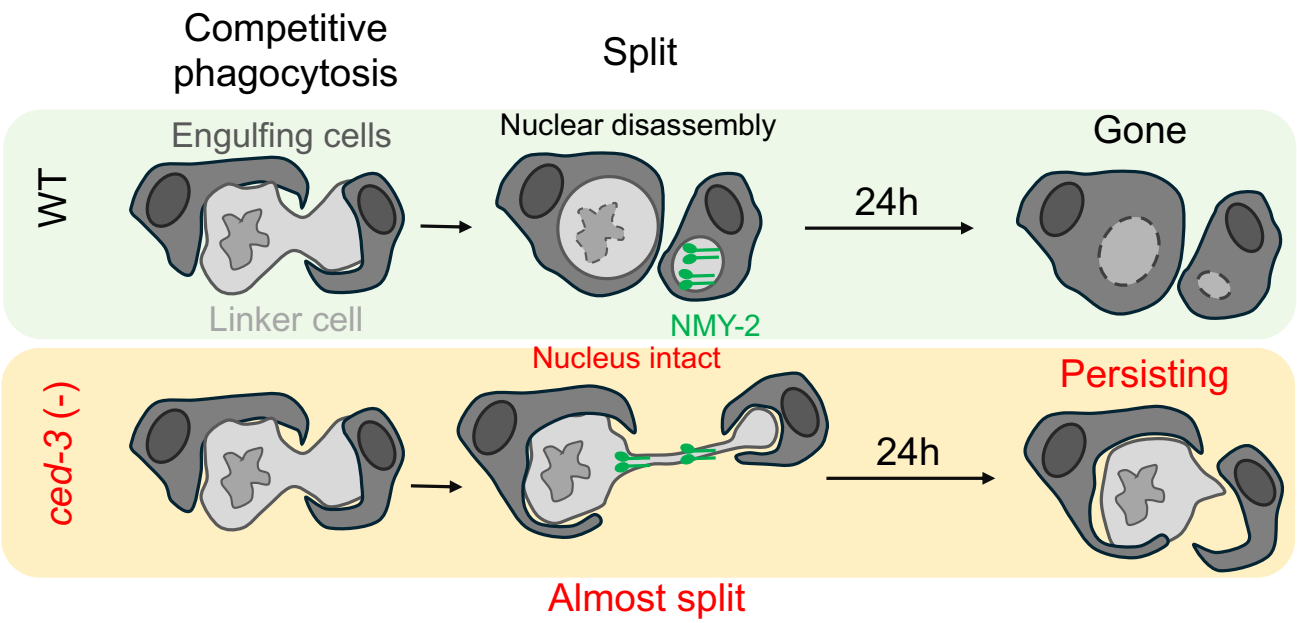

Figure 7. Model for CED-3 role in linker cell removal.

References

1. Ghose P, Shaham S. Cell death in animal development. Development. 2020;147(14). PMC7390631.
2. Horowitz LB, Shaham S. Apoptotic and Nonapoptotic Cell Death in Caenorhabditis elegans Development. Annu Rev Genet. 2024;58(1):113-34.
3. Kutscher LM, Shaham S. Non-apoptotic cell death in animal development. Cell Death Differ. 2017;24(8):1326-36. PMC5520451.
4. Basnakian AG, Moore CL. Apoptotic DNase network: Mutual induction and cooperation among apoptotic endonucleases. J Cell Mol Med. 2021;25(14):6496-9. PMC8278086.
5. Stanfield GM, Horvitz HR. The ced-8 gene controls the timing of programmed cell deaths in C. elegans. Mol Cell. 2000;5(3):423-33.
6. Suzuki J, Imanishi E, Nagata S. Exposure of phosphatidylserine by Xk-related protein family members during apoptosis. J Biol Chem. 2014;289(44):30257-67. PMC4215210.
7. Doran AC, Yurdagul A, Jr., Tabas I. Efferocytosis in health and disease. Nat Rev Immunol. 2020;20(4):254-67. PMC7667664.
8. Fazeli G, Levin-Konigsberg R, Bassik MC, Stigloher C, Wehman AM. A BORC-dependent molecular pathway for vesiculation of cell corpse phagolysosomes. Curr Biol. 2023;33(4):607-21 e7. PMC9992095.
9. Kolli S, Kline CJ, Rad KM, Wehman AM. Phagolysosomes break down the membrane of a non-apoptotic corpse independent of macroautophagy. PLoS One. 2024;19(11):e0306435. PMC11581207.
10. Sulston JE, Horvitz HR. Post-embryonic cell lineages of the nematode, Caenorhabditis elegans. Dev Biol. 1977;56(1):110-56.
11. Sulston JE, Schierenberg E, White JG, Thomson JN. The embryonic cell lineage of the nematode Caenorhabditis elegans. Dev Biol. 1983;100(1):64-119.
12. Ellis HM, Horvitz HR. Genetic control of programmed cell death in the nematode C. elegans. Cell. 1986;44(6):817-29.
13. Yuan J, Shaham S, Ledoux S, Ellis HM, Horvitz HR. The C. elegans cell death gene ced-3 encodes a protein similar to mammalian interleukin-1 beta-converting enzyme. Cell. 1993;75(4):641-52.
14. Abraham MC, Lu Y, Shaham S. A morphologically conserved nonapoptotic program promotes linker cell death in Caenorhabditis elegans. Dev Cell. 2007;12(1):73-86.
15. Kimble J, Hirsh D. The postembryonic cell lineages of the hermaphrodite and male gonads in Caenorhabditis elegans. Dev Biol. 1979;70(2):396-417.
16. Kutscher LM, Keil W, Shaham S. RAB-35 and ARF-6 GTPases Mediate Engulfment and Clearance Following Linker Cell-Type Death. Dev Cell. 2018;47(2):222-38 e6. PMC6200590.
17. Denning DP, Hatch V, Horvitz HR. Both the caspase CSP-1 and a caspase-independent pathway promote programmed cell death in parallel to the canonical pathway for apoptosis in Caenorhabditis elegans. PLoS Genet. 2013;9(3):e1003341. PMC3591282.
18. Kinet MJ, Malin JA, Abraham MC, Blum ES, Silverman MR, Lu Y, et al. HSF-1 activates the ubiquitin proteasome system to promote non-apoptotic developmental cell death in C. elegans. Elife. 2016;5. PMC4821803.

19. Blum ES, Abraham MC, Yoshimura S, Lu Y, Shaham S. Control of nonapoptotic developmental cell death in Caenorhabditis elegans by a polyglutamine-repeat protein. Science. 2012;335(6071):970-3. PMC3858082.
20. Malin JZ, Shaham S. Chapter One - Cell Death in C. elegans Development. In: Steller H, editor. Current Topics in Developmental Biology. 114: Academic Press; 2015. p. 1-42.
21. Imao T, Nagata S. Apaf-1- and Caspase-8-independent apoptosis. Cell Death Differ. 2013;20(2):343-52. PMC3554337.
22. Keil W, Kutscher LM, Shaham S, Siggia ED. Long-Term High-Resolution Imaging of Developing C. elegans Larvae with Microfluidics. Dev Cell. 2017;40(2):202-14. PMC5263027.
23. Botelho RJ, Teruel M, Dierckman R, Anderson R, Wells A, York JD, et al. Localized biphasic changes in phosphatidylinositol-4,5-bisphosphate at sites of phagocytosis. J Cell Biol. 2000;151(7):1353-68. PMC2150667.
24. Cheng S, Wang K, Zou W, Miao R, Huang Y, Wang H, et al. PtdIns(4,5)P(2) and PtdIns3P coordinate to regulate phagosomal sealing for apoptotic cell clearance. J Cell Biol. 2015;210(3):485-502. PMC4523610.
25. Guo S, Kemphues KJ. A non-muscle myosin required for embryonic polarity in Caenorhabditis elegans. Nature. 1996;382(6590):455-8.
26. Shelton CA, Carter JC, Ellis GC, Bowerman B. The nonmuscle myosin regulatory light chain gene mlc-4 is required for cytokinesis, anterior-posterior polarity, and body morphology during Caenorhabditis elegans embryogenesis. J Cell Biol. 1999;146(2):439-51. PMC3206578.
27. Tamaoki T, Nomoto H, Takahashi I, Kato Y, Morimoto M, Tomita F. Staurosporine, a potent inhibitor of phospholipid/Ca++dependent protein kinase. Biochem Biophys Res Commun. 1986;135(2):397-402.
28. Philpott KL, McCarthy MJ, Becker D, Gatchalian C, Rubin LL. Morphological and biochemical changes in neurons: apoptosis versus mitosis. Eur J Neurosci. 1996;8(9):1906-15.
29. Weil M, Jacobson MD, Coles HS, Davies TJ, Gardner RL, Raff KD, et al. Constitutive expression of the machinery for programmed cell death. J Cell Biol. 1996;133(5):1053-9. PMC2120862.
30. Weaver BP, Weaver YM, Omi S, Yuan W, Ewbank JJ, Han M. Non-Canonical Caspase Activity Antagonizes p38 MAPK Stress-Priming Function to Support Development. Dev Cell. 2020;53(3):358-69 e6. PMC7641037.
31. Boice AG, Lopez KE, Pandita RK, Parsons MJ, Charendoff CI, Charaka V, et al. Caspase-2 regulates S-phase cell cycle events to protect from DNA damage accumulation independent of apoptosis. Oncogene. 2022;41(2):204-19. PMC8738157.
32. Sumida K, Doi T, Obayashi K, Chiba Y, Nagasaka S, Ogino N, et al. Caspase-4 has a role in cell division in epithelial cells through actin depolymerization. Biochem Biophys Res Commun. 2024;695:149394.
33. Connolly P, Garcia-Carpio I, Villunger A. Cell-Cycle Cross Talk with Caspases and Their Substrates. Cold Spring Harb Perspect Biol. 2020;12(6). PMC7263087.
34. Nigg EA. Assembly and cell cycle dynamics of the nuclear lamina. Semin Cell Biol. 1992;3(4):245-53.

35. Wang K, Okada H, Bi E. Comparative Analysis of the Roles of Non-muscle Myosin-IIs in Cytokinesis in Budding Yeast, Fission Yeast, and Mammalian Cells. Front Cell Dev Biol. 2020;8:593400. PMC7710916.
36. Arama E, Baena-Lopez LA, Fearnhead HO. Non-lethal message from the Holy Land: The first international conference on nonapoptotic roles of apoptotic proteins. FEBS J. 2021;288(7):2166-83.
37. Dehkordi MH, Munn RGK, Fearnhead HO. Non-Canonical Roles of Apoptotic Caspases in the Nervous System. Front Cell Dev Biol. 2022;10:840023. PMC8904960.
38. Hollville E, Deshmukh M. Physiological functions of non-apoptotic caspase activity in the nervous system. Semin Cell Dev Biol. 2018;82:127-36. PMC5988915.
39. Kutscher LM, Shaham S. Forward and reverse mutagenesis in C. elegans. WormBook. 2014:1-26. PMC4078664.
40. Kamath RS, Ahringer J. Genome-wide RNAi screening in Caenorhabditis elegans. Methods. 2003;30(4):313-21.
41. Lundquist EA, Reddien PW, Hartwieg E, Horvitz HR, Bargmann CI. Three C. elegans Rac proteins and several alternative Rac regulators control axon guidance, cell migration and apoptotic cell phagocytosis. Development. 2001;128(22):4475-88.